A spatial-skew model for extreme values

May 14, 2015

1 Introduction

In most climatological applications, researchers are interested in learning about the average behavior of different climate variables (e.g. ozone, temperature, rainfall). However, averages are not adequate to prepare for the unusual events that only happen once every 100 years. For example, it is important to have an idea of how much rain will come in a 100-year flood in order to construct strong enough river levees to protect lands from flooding. To accurately estimate the risk associated with such rare events, it is imperative to use statistical models designed for extreme values. Given that many of these applications demonstrate some level of spatial and temporal dependence, there is a growing interest in spatio-temporal methods for extreme values.

Traditionally, spatial methods for extreme values analysis are conducted from one of two perspectives. The first of these is based on the convergence of the maximums of independent stochastic processes to a max-stable process (de Haan and Ferreira, 2006). Finite dimensional realizations of a max-stable process follow a generalized extreme value distribution (Cooley et al., 2012). One drawback to a block-maxima approach is that information is lost by discarding all but the most extreme observations in a block. Furthermore, in using multivariate block-maxima methods, the observations in the vector of block maxima rarely occur simultaneously (Coles, 2001). The other perspective incorporates a peaks-over-threshold approach. This methodology requires selecting a threshold, beyond which, the data are assumed to be considered extreme. Recently, threshold methods have become a popular choice through censored pairwise composite likelihoods (Wadsworth and Tawn, 2012; Thibaud et al., 2013; Thibaud and Opitz, 2013; Huser and Davison, 2014).

Unlike multivariate normal distributions, multivariate extreme value distributions are challenging to

1

use directly because closed-form expressions for the density in more than two dimensions are complicated (Coles and Tawn, 1991). One exception to this is the Brown-Resnick process, a process for which it is possible to conduct inference in d-dimensions (Wadsworth and Tawn, 2013; Engelke et al., 2014). Extreme value distributions based on the skew-t distribution also permit modeling of extreme values in higher dimensions (Padoan, 2011). This limitation has led to the development of pairwise composite likelihood methods to model spatially dependent extremes (Padoan et al., 2010; Blanchet and Davison, 2011; Huser, 2013). Bayesian methods have also been proposed using hierarchical models with positive stable random effects (Reich and Shaby, 2012).

Despite these challenges, the spatial modeling of extremes is important because it provides a mechanism by which we can borrow information about extreme events across space. There are two primary goals when modeling spatial extremes. The first of these goals is to understand the marginal behavior at sites, and the second is to describe the asymptotic dependence between sites. In many cases, these are done separately; however, with the development of pairwise composite likelihoods and Bayesian methods, it is resonable to model both simultaneously. One challenge to estimating the asymptotic dependence is that the observed extremal dependence may not be the same as the limiting dependence (Davison and Gholamrezaee, 2012). Furthermore, in a spatial setting, it may be desirable to have varying degrees of asymptotic dependence based upon the distance between two sites (Wadsworth and Tawn, 2012).

One way around the multi-dimensional limitations of multivariate extreme value distributions is to use skew elliptical distributions to model dependent extreme values (Genton, 2004; Zhang and El-Shaarawi, 2010; Padoan, 2011). For example, the skew-normal and skew-t distribution offer a flexible way to handle non-symmetric data within a framework of multivariate normal and multivariate t distributions. As with multivariate Gaussian distributions, the multivariate skew-normal distribution demonstrates asymptotic independence. Conversely both the multivariate t and skew-t distributions demonstrate asymptotic depen-

dence (Padoan, 2011). Additionally, the limiting distribution of the maxima of skew-t random vectors is the extremal skew-t distribution (Padoan, 2011) of which the extremal-t (Opitz, 2013) is a special case.

In many cases, the goal of analyzing extreme values is to understand the behavior of very rare events; however, we take a slightly different approach that is motivated by assessing ozone compliance. A site is said to be in compliance if the fourth highest daily maximum 8-hour concentration averaged over 3 years does not exceed 75 parts per billion. Because this value typically occurs during the summer months, the fourth highest daily maximum is roughly equivalent to modeling the 95th quantile for ozone for the summer or 99th quantile for the year. These high quantiles are extreme in the sense that they are unusual for a given year, but they are not extreme in the sense that we are always guaranteed to observe this quantile level every year at each site by definition.

In this paper, we present a new spatio-temporal model based on the skew-t process that is informed by two concepts from extreme value analysis. Specifically, our contribution is to incorporate thresholding and random spatial partitions using a multivariate skew-t distribution. The advantage of using a thresholded model as opposed to a non-thresholded model is that is allows for the tails of the distribution to inform the predictions in the tails (DuMouchel, 1983). The random spatial partitions are similar to the method used by Kim et al. (2005) for non-stationary Gaussian data, and they alleviate the asymptotic spatial dependence present in the skew-t distribution for sites that are far apart. Finally, our model allows for inference and predictions using the full likelihood with computing on the order of Gaussian models for large space-time datasets.

The paper is organized as follows. Section 2 is a brief review of the spatial skew-t process. In Section 3.3, we build upon the traditional skew-t by incorporating censoring to focus on tails, partitioning to remove long-range asymptotic dependence, and extending the model to space-time data. The computing is described in Section 4. In Section 5, we present a simulation study that examines the predictive capabilities of this

69 model compared with a naïve Gaussian method. We then compare our method to Gaussian and max-stable

70 methods with a data analysis of ozone measurements from throughout the US in section 6. The final section

71 provides brief discussion and direction for future research.

2 Spatial skew processes

73 Many types of data demonstrate some level of skewness and therefore should be modeled with distributions

74 that allow for asymmetry. The skew-elliptical family of distributions provides models that are mathemati-

75 cally tractable while introducing a slant parameter to account for asymmetric data (Genton, 2004). A brief

76 review of the additive process by which a skew-t process is created is given here.

2.1 Skew-t process

78 Let $Y(\mathbf{s})$ be the observation at spatial location $\mathbf{s} = (s_1, s_2)$. The spatial skew-t process can be written

$$Y(\mathbf{s}) = \mathbf{X}(\mathbf{s})^T \boldsymbol{\beta} + \lambda \sigma |z| + \sigma v(\mathbf{s}) \tag{1}$$

79 where $\mathbf{X}(\mathbf{s})$ is a set of spatial covariates at site $\mathbf{s}$, $\boldsymbol{\beta}$ is the vector of regression parameters, $\lambda \in \mathcal{R}$ is a

80 parameter controlling skew, $z \sim N(0, 1)$, $\sigma^2 \sim \mathrm{IG}(a, b)$ is an inverse gamma random variable, and $v(\mathbf{s})$ is

81 a spatial Gaussian process with mean zero and variance one.

82   Let $\mathbf{Y} = [Y(\mathbf{s}_1), \ldots, Y(\mathbf{s}_n)]^T$ be a set of observations at a finite collection of locations $\mathbf{s}_1, \ldots, \mathbf{s}_n$. After

83 marginalizing over both z and σ,

$$\mathbf{Y} \sim \mathrm{ST}_n(\mathbf{X}\boldsymbol{\beta}, \boldsymbol{\Omega}, \boldsymbol{\alpha}, 2a), \tag{2}$$

84 that is, $\mathbf{Y}$ follows an n-dimensional skew-t distribution with location $\mathbf{X}\boldsymbol{\beta}$, correlation matrix $\boldsymbol{\Omega}$, slant param-

4

eters $\boldsymbol{\alpha}$ and degrees of freedom $2a$, where $\mathbf{X} = [\mathbf{X}(\mathbf{s}_1)^T, \dots, \mathbf{X}(\mathbf{s}_n)^T]$, $\boldsymbol{\Omega} = \boldsymbol{\omega}\bar{\boldsymbol{\Omega}}\boldsymbol{\omega}$, $\boldsymbol{\omega} = \text{diag}\left(\frac{1}{\sqrt{ab}}, \dots, \frac{1}{\sqrt{ab}}\right)$,

$\bar{\boldsymbol{\Omega}} = (\boldsymbol{\Sigma} + \lambda^2 \mathbf{1}\mathbf{1}^T)$, $\boldsymbol{\Sigma}$ is a positive definite correlation matrix, $\boldsymbol{\alpha} = \lambda(1 + \lambda^2 \mathbf{1}^T \boldsymbol{\Sigma}^{-1} \mathbf{1})^{-1/2} \mathbf{1}^T \boldsymbol{\Sigma}^{-1}$ is a

vector of slant parameters. Although $\boldsymbol{\Sigma}$ can be any positive definite correlation matrix, we choose to use the

stationary isotropic Matérn correlation with

$$\text{cor}[v(\mathbf{s}), v(\mathbf{t})] = \gamma I(\mathbf{s} = \mathbf{t}) + (1 - \gamma)\frac{1}{\Gamma(\nu)2^{\nu-1}}\left(\sqrt{2\nu}\frac{h}{\rho}\right)^{\nu} K_{\nu}\left(\sqrt{2\nu}\frac{h}{\rho}\right) \tag{3}$$

where ρ is the spatial range, ν is the smoothness, γ is the proportion of variance accounted for by the

spatial variation, K_{ν} is a modified Bessel function of the second kind, and $h = ||\mathbf{s} - \mathbf{t}||$. This process is

desirable because of its flexible tail that is controlled by the skewness parameter λ and degrees of freedom

$2a$. Furthermore, the marginal distributions at each location also follow a univariate skew-t distribution (**?**).

2.2 Extremal dependence

Our interest lies in spatial dependence in the tail of the skew-t process. One measure of extremal dependence

is the χ statistic (Padoan, 2011). For a stationary and isotropic spatial process, the χ statistic for two location

$\mathbf{s}$ and $\mathbf{t}$ separated by distance $h = ||\mathbf{s} - \mathbf{t}||$ is

$$\chi(h) = \lim_{c \to \infty} \Pr[Y(\mathbf{s}) > c | Y(\mathbf{t}) > c]. \tag{4}$$

If $\chi(h) = 0$, then observations are asymptotically independent at distance h. For Gaussian processes,

$\chi(h) = 0$ regardless of the distance, so they are not suitable for modeling spatially-dependent extremes.

Unlike the Gaussian process, the skew-t process is asymptotically dependent. However, one problem with

the spatial skew-t process is that $\lim_{h \to \infty} \chi(h) > 0$ (see Appendix A.4 for a proof). This occurs because

all observations, both near and far, share the same z and σ terms. Therefore, this long-range dependence

5

feature of the skew-t process is not ideal for spatial analysis of large geographic regions where we expect

only local spatial dependence. The explicit expression for $\chi(h)$ is given in Appendix A.4.

3 Spatiotemporal skew-t model for extremes

In this section, we propose extensions to the skew-t process to model spatial extremes over a large geo-

graphic region by introducing censoring to focus on tail behavior and a random partition to remove long-

range asymptotic dependence. For notational convenice, we introduce the model for a single replication,

and then extend this model to the spatiotemporal setting in Section 3.3.

3.1 Censoring to focus on the tails

To avoid bias in estimating tail parameters, we model censored data. Let

$$
\widetilde{Y}(\mathbf{s}) = \begin{cases} Y(\mathbf{s}) & \delta(\mathbf{s}) = 1 \\ \\ T & \delta(\mathbf{s}) = 0 \end{cases} \tag{5}
$$

be the censored observation at site $\mathbf{s}$ where $Y(\mathbf{s})$ is the uncensored observation, $\delta(\mathbf{s}) = I[Y(\mathbf{s}) > T]$, and T

is a pre-specified threshold value. Then, assuming the uncensored data $Y(\mathbf{s})$ are observations from a skew-t

process, we update values censored below the threshold using standard Bayesian missing data methods as

described in Section 4.

3.2 Partitioning to remove long-range asymptotic dependence

We handle the problem of long-range asymptotic dependence with a random partition. As discussed in

Section 2, the source of long-range dependence is the shared z and σ. Therefore, to alleviate this dependence,

6

118   we allow z and σ to vary by site. The model becomes

$$Y(\mathbf{s}) = \mathbf{X}(\mathbf{s})^T \boldsymbol{\beta} + \lambda \sigma(\mathbf{s})|z(\mathbf{s})| + \sigma(\mathbf{s})v(\mathbf{s}). \tag{6}$$

119   Let $\mathbf{w} = (w_1, w_2)$ be the location of a spatial knot. To model spatial variation, consider a set of spatial knots

120   $\mathbf{w}_1, \ldots, \mathbf{w}_K$ from a homogeneous Poisson process with intensity μ over spatial domain $\mathcal{D} \in \mathcal{R}^2$. The knots

121   define a random partition of $\mathcal{D}$ by subregions $P_1, \ldots, P_K$ defined as

$$P_k = \{\mathbf{s} : k = \arg\min_\ell ||\mathbf{s} - \mathbf{w}_\ell||\}. \tag{7}$$

122   All $z(\mathbf{s})$ and $\sigma(\mathbf{s})$ for sites in subregion k are assigned common values

$$z(\mathbf{s}) = z_k \quad \text{and} \quad \sigma(\mathbf{s}) = \sigma_k \tag{8}$$

123   and the z_k and σ_k^2 are distributed as $z_k \overset{iid}{\sim} N(0, 1)$ and $\sigma^2 \overset{iid}{\sim} \text{IG}(a, b)$ where IG is the distribution function

124   of an inverse gamma random variable. So, within each partition, $Y(\mathbf{s})$ follows the spatial skew-t process

125   defined in Section 2. Across partitions, the $Y(\mathbf{s})$ remain correlated via the correlation function for $v(\mathbf{s})$

126   because $v(\mathbf{s})$ spans all partitions.

127   When incorporating the random partition, conditional on knots $\mathbf{w}_1, \ldots, \mathbf{w}_K$, the χ statistic for two sites

128   $\mathbf{s}$ and $\mathbf{t}$ in partitions k_s and k_t respectively is

$$\chi(h) = I(k_s = k_t)\chi_{\text{skew-}t}(h) + I(k_s \neq k_t)\chi_{\text{Gaus}}(h)$$

$$= I(k_s = k_t)\chi_{\text{skew-}t}(h) \tag{9}$$

129   where $I(\cdot)$ is an indicator function, $\chi_{\text{skew-}t}(h)$ is the χ statistic for a skew-t process, $\chi_{\text{Gaus}}(h)$ is the χ statistic
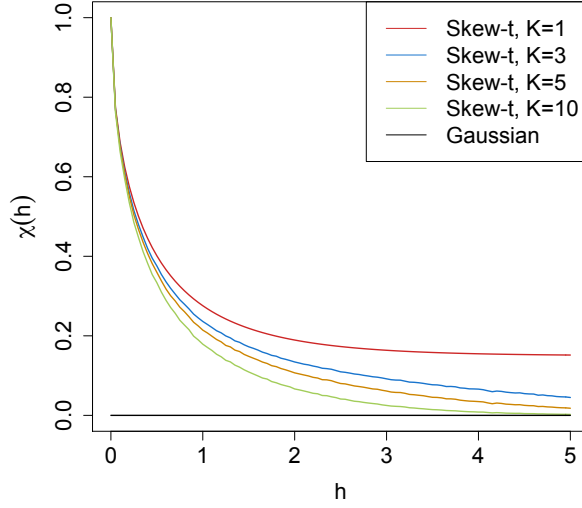
Figure 1: $\chi(h)$ for $K = 1, 3, 5$, and 10 knots as a function of distance.

for a Gaussian process, and $h = ||\mathbf{s} - \mathbf{t}||$. Therefore, sites in different subregions are asymptotically inde-

pendent because $\chi_{\text{Gaus}}(h) = 0$ for all h. Marginally, over the knots $\mathbf{w}_1, \ldots, \mathbf{w}_K$, $\chi(h) = \pi(h)\chi_{\text{skew}-t}(h)$,

where $\pi(h) = \Pr(k_s = k_t)$ is the probability that two sites separated by distance h are in the same partition.

So, to show that $\lim_{h\to\infty} \chi(h) = 0$, we need only know that $\lim_{h\to\infty} \pi(h) = 0$. A proof of this is given in

Appendix A.3.

In Figure 1, we give $\chi(h)$ for $K = 1, 3, 5, 10$ partitions for a skew-t distribution with $\alpha = 10$, and

3 degrees of freedom. To estimate $\pi(h)$, we generate 500 sites uniformly over the unit-square. We then

randomly generate 400 different sets of partitions using $K = 3$, 5, and 10. For each set of knots, we

take $\pi(h)$ to be the proportion of sites in the same partition that are separated by distance h. This plot

demonstrates how partitioning helps to reduce extremal dependence as h increases.

3.3 Extension to space-time data

When using daily measurements, the assumption of temporal independence is inappropriate. There are several places where temporal dependence could be incorporated in the model, including the residual $v_t(\mathbf{s})$. However, we choose to allow for temporal dependence in the $\mathbf{w}$, z, and σ terms because these terms dictate the tail behavior which is our primary focus. In this section, we extend (6) to the spatiotemporal setting. Let

$$Y_t(\mathbf{s}) = \mathbf{X}_t(\mathbf{s})^T \boldsymbol{\beta} + \lambda \sigma_t(\mathbf{s})|z_t(\mathbf{s})| + \sigma_t(\mathbf{s}) v_t(\mathbf{s}), \tag{10}$$

where $t \in \{1, \ldots, T\}$ denotes the day of each observation. Let $\mathbf{w}_{tk} = (w_{tk1}, w_{tk2})$ be a spatial knot on day t, and let $w_{t1}, \ldots, w_{tK}$ be a collection of spatial knots on day t. As in section 3.2, these knots define a daily partition $P_{t1}, \ldots, P_{tK}$, and for $\mathbf{s} \in P_{tk}$,

$$z_t(\mathbf{s}) = z_{tk} \quad \text{and} \quad \sigma_t(\mathbf{s}) = \sigma_{tk}. \tag{11}$$

We use an AR(1) time series model for w_{tk}, z_{tk}, and σ_{tk}. The time series model must be specified after a transformation to preserve the skew-t process at each time point. For each time-varying parameter, we transform to obtain a standard normal marginal distribution, place a Gaussian prior with autocorrelation on the transformed parameter, and then transform back to obtain the marginal distribution required to preserve the skew-t process. We first transform the spatial knots from $\mathcal{D}$ to $\mathcal{R}^2$ as follows. Let

$$w_{tki}^* = \Phi^{-1}\left[\frac{w_{tki} - \min(\mathbf{s}_i)}{\max(\mathbf{s}_i) - \min(\mathbf{s}_i)}\right], \quad i = 1, 2 \tag{12}$$

where Φ is a univariate standard normal density function, and $\mathbf{s}_i = [s_{1i}, \ldots, s_{ni}]$. Then the transformed knots $\mathbf{w}_{tk}^* \in \mathcal{R}^2$. We use a copula on $\sigma_t^2(\mathbf{s})$ to ensure that the marginal distributions of $\sigma_t^2(\mathbf{s})$ are inverse

9

gamma. Let

$$\sigma_t^{2*}(\mathbf{s}) = \Phi^{-1}\left\{\mathrm{IG}[\sigma_t^2(\mathbf{s})]\right\} \tag{13}$$

where IG is defined as before. We also use a copula on $z_t(\mathbf{s})$ to ensure that the marginal distributions of $z_t(\mathbf{s})$ are half-normal. Let

$$z_t^*(\mathbf{s}) = \Phi^{-1}\left\{\mathrm{HN}[z_t(\mathbf{s})]\right\} \tag{14}$$

where HN is the distribution function of a half-normal random variable. The AR(1) process for each tail parameter is $\mathbf{w}_{1k}^* \sim N_w(0,1)$, $z_{1k}^* \sim N(0, \sigma_{1k}^2)$, $\sigma_{1k}^{2*} \sim N(0,1)$, and for $t > 1$ the time series is modeled as

$$\mathbf{w}_{tk}^* | \mathbf{w}_{t-1,k}^* \sim N_2\left[\phi_w \mathbf{w}_{t-1,k}^*, (1 - \phi_w^2)\right] \tag{15}$$

$$z_{tk}^* | z_{t-1,k}^* \sim N\left[\phi_z z_{t-1,k}^*, \sigma_{tk}^2(1 - \phi_z^2)\right] \tag{16}$$

$$\sigma_{tk}^{2*} | \sigma_{t-1,k}^{2*} \sim N\left[\phi_\sigma \sigma_{t-1,k}^{2*}, (1 - \phi_\sigma^2)\right] \tag{17}$$

where $|\phi_w|, |\phi_z|, |\phi_\sigma| < 1$. These are stationary time series models with marginal distributions $\mathbf{w}_k^* \sim N_2(0,1)$, $z_k^* \sim N(0, \sigma_k^2)$, and $\sigma_k^{2*} \sim N(0,1)$. After transformation back to the original space, $\mathbf{w}_{tk} \sim \mathrm{Unif}(\mathcal{D})$, $z_{tk} \sim HN(0, \sigma_{tk}^2)$ $\sigma_{tk}^2 \sim \mathrm{IG}(a, b)$. For each day, the model is identical to the spatial-only model in (6) by construction.

4 Computation

First, we impute values below the threshold. Then, we update model parameters, Θ, using Metropolis Hastings or Gibbs sampling when appropriate. Finally, we make spatial predictions using conditional mul-

10

tivariate normal results and the fact that the distribution of $Y_t(\mathbf{s}) \mid \Theta, z(\mathbf{s})$ is the usual multivariate normal

distribution with a Matérn spatial covariance structure.

We can use Gibbs sampling to update $Y_t(\mathbf{s})$ for censored observations that are below the threshold T. After conditioning on λ, $z_t(\mathbf{s})$ and non-censored observations, $Y_t(\mathbf{s})$ has truncated normal full conditionals. So we sample $Y_t(\mathbf{s}) \sim N_{(-\infty, T)}(\mathbf{X}_t^T(\mathbf{s})\beta + \lambda|z_t(\mathbf{s})|, \boldsymbol{\Sigma})$. After imputing the censored observations, we update the model parameters. To update the model parameters, we use standard Gibbs updates for parameters when possible. In the case Gibbs sampling is not possible, parameters are updated using a random-walk Metropolis Hastings algorithm. See Appendices A.1 and A.2 for details regarding the MCMC. The final step of the computation is to use Bayesian Kriging to generate a predictive distribution for $Y_t(\mathbf{s}^*)$ at prediction location $\mathbf{s}^*$. This step is similar to the imputation for censored observations except that the full conditionals are no longer truncated at T.

4.1 Hierarchical model

Conditioned on $z_{tk}(\mathbf{s})$, $\sigma_{tk}^2(\mathbf{s})$, and P_{tk}, the marginal distributions are Gaussian and the joint distribution multivariate Gaussian. However, we do not fix the partitions, they are treated as unknown and updated in the MCMC. We model this with a Bayesian hierarchical model as follows. Let $\mathbf{w}_{t1}, \ldots, \mathbf{w}_{tK}$ be a set of daily

spatial knots in a spatial domain of interest, $\mathcal{D}$, and P_{tk} as defined in (7). Then

$$Y_t(\mathbf{s}) \mid z_t(\mathbf{s}), \sigma_t^2(\mathbf{s}), P_{tk}, \Theta = \mathbf{X}_t(\mathbf{s})^T \beta + \lambda |z_t(\mathbf{s})| + \sigma_t(\mathbf{s}) v_t(\mathbf{s}) \tag{18}$$

$$z_t(\mathbf{s}) = z_{tk} \text{ if } \mathbf{s} \in P_{tk}$$

$$\sigma_t^2(\mathbf{s}) = \sigma_{tk}^2 \text{ if } \mathbf{s} \in P_{tk}$$

$$\lambda = \lambda_1 \lambda_2$$

$$\lambda_1 = \begin{cases} +1 & \text{w.p. } 0.5 \\ -1 & \text{w.p. } 0.5 \end{cases}$$

$$\lambda_2^2 \sim IG(a, b)$$

$$v_t(\mathbf{s}) \mid \Theta \sim \text{Matérn}(0, \Sigma)$$

$$z_{tk}^* \mid z_{t-1,k}^*, \sigma_{tk}^2 \sim N(\phi_z z_{t-1,k}^*, \sigma_{tk}^2(1 - \phi_z^2))$$

$$\sigma_{tk}^{2*} \mid \sigma_{t-1,k}^{2*} \sim N(\phi_\sigma \sigma_{t-1,k}^{2*}, (1 - \phi_\sigma^2))$$

$$\mathbf{w}_{tk}^* \mid \mathbf{w}_{t-1,k}^* \sim N_2(\phi_w \mathbf{w}_{t-1,k}^*, (1 - \phi_w^2))$$

where $\Theta = \{\rho, \nu, \gamma\, \lambda, \beta\}$, and Σ is a Matérn covariance matrix as described in Section 2.1. We parameterize $\lambda = \lambda_1 \lambda_2$ to help with convergence in the MCMC.

5 Simulation study

In this section, we conduct a simulation study to investigate how the number of partitions and the level of thresholding impact the accuracy of predictions made by the model.

12

5.1 Design

For all simulation designs, we generate data from the model in Section 3.2 using $n_s = 144$ sites and $n_t = 50$ independent days. The sites are generated Uniform$([0, 10] \times [0, 10])$. We generate data from 5 different simulation designs:

1. Gaussian marginal, $K = 1$ knot

2. Skew-t marginal, $K = 1$ knots

3. Skew-t marginal, $K = 5$ knots

4. Max-stable

5. Transformation below $T = q(0.80)$

In the first three designs, the $v_t(\mathbf{s})$ terms are generated using a Matérn covariance with smoothness parameter $\nu = 0.5$ and spatial range $\rho = 1$. For the covariance matrices in designs $1 - 3$, the proportion of the variance accounted for by the spatial variation is $\gamma = 0.9$ while the proportion of the variance accounted for by the nugget effect is 0.1. In the first design, $\sigma^2 = 2$ is used for all days which results in a Gaussian distribution. For designs 2 and 3, $\sigma_{tk}^2 \overset{iid}{\sim} \text{IG}(3, 8)$ to give a t distribution with 6 degrees of freedom. For designs 1, we set $\lambda = 0$. For designs 2 and 3, $\lambda = 3$ was used as to simulate moderate skewness, and the z_t are generated as described in (8). In the fourth design, we generate from a spatial max-stable distribution (Reich and Shaby, 2012). In this design, data have marginal distributions that follow a generalized extreme value distribution with parameters $\mu = 1, \sigma = 1, \xi = 0.2$. In this model, a random effect is used to induce spatial dependence using 144 spatial knots on a regular lattice in the square $[1, 9] \times [1, 9]$. For this setting, we set $\gamma = 0.5$. In the final design, we generate $\tilde{y}$ using the setting from design two, and then consider the data

$$
y = \begin{cases} \tilde{y}, & \tilde{y} > T \\ T \exp\{\tilde{y} - T\}, & \tilde{y} \leq T \end{cases} \tag{19}
$$

13

where $T = q(0.80)$ is the 80th sample quantile of the data. In all five designs, the mean $\mathbf{X}^T\boldsymbol{\beta} = 10$ is assumed to be constant across space.

$M = 50$ data sets are generated for each design. For each data set we fit the data using five models

1. Gaussian marginal, $K = 1$ knots

2. Skew-t marginal, $K = 1$ knots, $T = -\infty$

3. Symmetric-t marginal, $K = 1$ knots, $T = q(0.80)$

4. Skew-t marginal, $K = 5$ knots, $T = -\infty$

5. Symmetric-t marginal, $K = 5$ knots, $T = q(0.80)$

where $q(0.80)$ is the 80th sample quantile of the data. The design matrix $\mathbf{X}$ includes an intercept with a first-order spatial trend with priors of $\beta_{\text{int}}, \beta_{\text{lat}}, \beta_{\text{long}}, \overset{iid}{\sim} \text{N}(0, 10)$. The spatial covariance parameters have priors $\log(\nu) \sim \text{N}(-1.2, 1)$, $\gamma \sim \text{Unif}(0, 1)$, $\rho \sim \text{Unif}(15)$. The skewness parameter has prior $\lambda_2 \sim \text{IG}(0.1, 0.1)$. The residual variance terms have priors $\sigma_t^2(\mathbf{s}) \sim \text{IG}(0.1, 0.1)$. The knots have priors $\mathbf{w} \sim \text{Unif}(\mathcal{D})$. We do not include skewness for the thresholded models because it cannot be identified with only one tail worth of data, and we do not fit the data using the max-stable methods from Reich and Shaby (2012) because of the computational constraints. Each chain of the MCMC ran for 20000 iterations with a burn-in period of 10000 iterations. Parameters appear to converge properly; however, in the models with multiple partitions (i.e. models 4 and 5) it is hard to assess the convergence of $\mathbf{w}$, $z(\mathbf{s})$, and $\sigma^2(\mathbf{s})$ because of partition label switching throughout the MCMC.

5.2 Cross validation

Models were compared using cross validation with 100 sites used as training sites and 44 sites witheld for testing. The model was fit using the training set, and predictions were generated at the testing site locations. Because one of the primary goals of this model is to predict extreme events, we use Brier scores to select

14

the model that best fits the data (Gneiting and Raftery, 2007). The Brier score for predicting exceedance of a threshold c is given by $[e(c) - P(c)]^2$ where $e(c) = I[y > c]$ is an indicator function indicating that a test set value, y, has exceeded the threshold, c, and $P(c)$ is the predicted probability of exceeding c. We average the Brier scores over all test sites and days. For the Brier score, a lower score indicates a better fit.

5.3   Results

We compared the Brier scores for exceeding 4 different thresholds for each dataset. The thresholds used for the Brier scores are extreme quantiles from the simulated data for $q(0.90)$, $q(0.95)$, $q(0.98)$, and $q(0.99)$. Figure 2 gives the Brier score relative to the Brier score for the Gaussian method calculated as

$$\text{BS}_{\text{rel}} = \frac{\text{BS}_{\text{method}}}{\text{BS}_{\text{Gaussian}}}. \tag{20}$$

We analyzed the results for the simulation study using a Friedman test at $\alpha = 0.05$. If the Friedman test came back with a significant results, we conducted a Wilcoxon-Nemenyi-McDonald-Thompson test to see which methods had different results. The full results for the Wilcoxon-Nemenyi-McDonald-Thompson tests are given in Appendix A.5.

Figure 2 shows that when the data come from a Gaussian process, our methods perform comparably to the Gaussian method. For data settings with skew-t marginals (settings $2 - 3$), we find significant improvement over the Gaussian method. Furthermore in these data settings, we find the best performance occurs when the number of knots used in the method matches the number of knots used for data generation. The non-thresholded methods tend to outperform the thresholded methods, but this is not surprising given that the data are generated directly from the model used in the method. For the max-stable data, we see that for low-extreme quantiles, the Gaussian method performs better, for more extreme quantiles, the single-partition method, both thresholded and non-thresholded, perform significantly better than the Gaussian. Finally, for
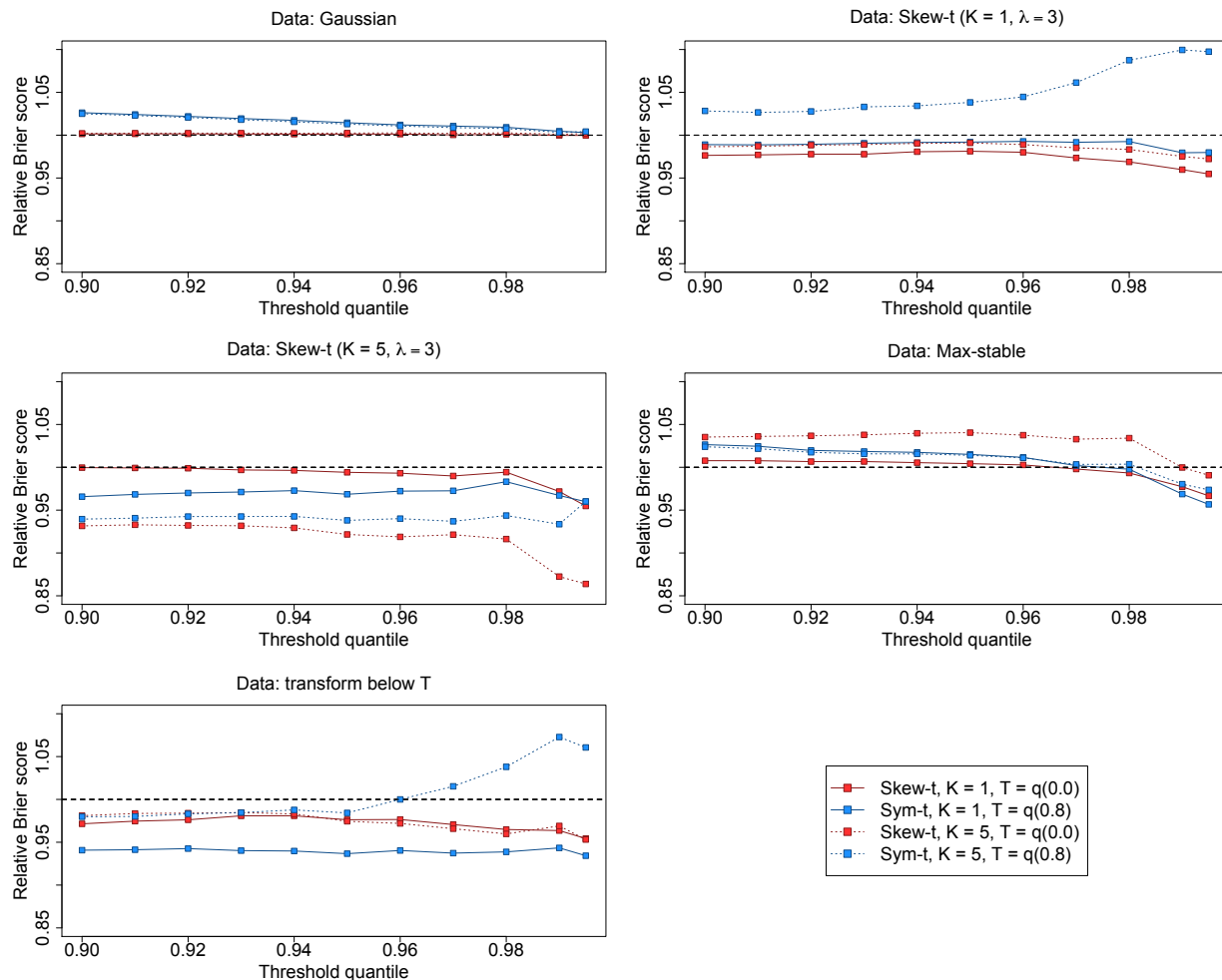
15

Figure 2: Brier scores relative to the Gaussian method for simulation study results. A ratio lower than 1 indicates that the method outperforms the Gaussian method.

setting 5, although the thresholded version of the single-partition model tends to perform the best across all

of the extreme quantiles, the difference between the thresholded and non-thresholded methods is no longer

significant in the more extreme quantiles.

6   Data analysis

To illustrate this method, we consider the daily maximum 8-hour ozone measurements for July 2005 at 1089

Air Quality System (AQS) monitoring sites in the United States as the response (see Figure 3). For each
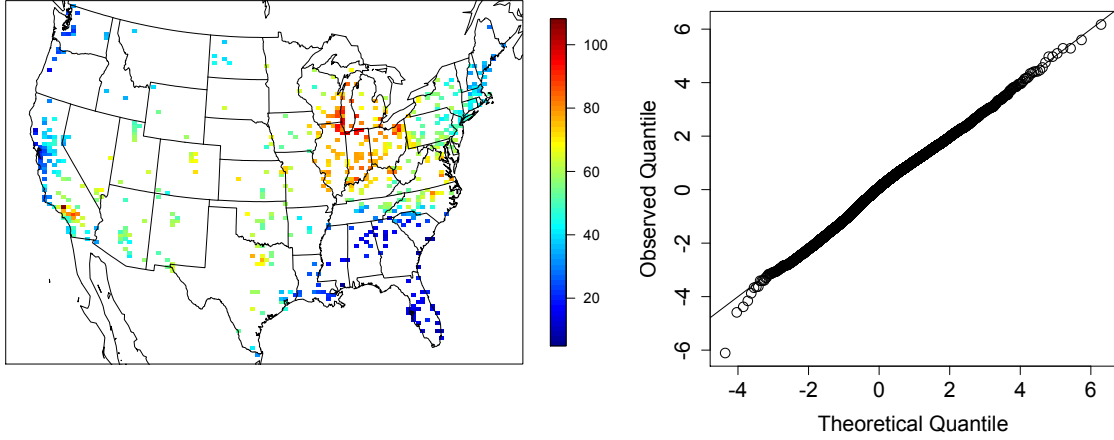
16

Figure 3: Ozone values on 10 July 2005 (left) Q-Q plot of the residuals (right)

site, we also have covariate information containing the estimated ozone from the Community Multi-scale

Air Quality (CMAQ) modeling system. Initially, we fit a linear regression assuming a mean function of

$$\mathbf{X}_t^T(\mathbf{s})\boldsymbol{\beta} = \beta_0 + \beta_1 \cdot \text{CMAQ}_t(\mathbf{s}). \tag{21}$$

The data from July 10 are shown in Figure 3 along with a Q-Q plot of the residuals compared to a skew-t

distribution with 10 d.f. and $\alpha = 1$. Exploratory data analysis indicates that there is dependence in the high

quantile levels of the residuals beyond what we expect in the case if independence.

6.1 Model comparisons

We fit the model using Gaussian and skew-t marginal distributions with $K = 1, 5, 6, 7, 8, 9, 10, 15$ partitions.

We choose to censor $Y(\mathbf{s})$ at $T = 0, 50$ (0.42 sample quantile), and 75 (0.92 sample quantile) ppb in order

to compare results from no, moderate, and high censoring. The upper threshold of 75 ppb was used because

the current air quality standard is based on exceedance of 75 ppb. As with the simuliation study, for models

with a threshold of $T = 75$, we use a symmetric-t marginal distribution. We also compare models with no

17

time series to models that include the time series. Finally, as a comparison to max-stable methods, we fit the model using the hierarchical max-stable model of Reich and Shaby (2012). All methods assume the mean function given in (21). To ensure that the max-stable method runs in a reasonable amount of time, we take a stratified sample of the sites to get 800 sites and consider this our new dataset. We conduct two-fold cross validation using 400 training sites and 400 validation sites as described in Section 5.2

Each chain of the MCMC ran for 30000 iterations with a burn-in period of 25000 iterations. Parameters appear to converge properly; however, as before, for models with multiple partitions it is hard to assess the convergence of $\mathbf{w}$, $z(\mathbf{s})$, and $\sigma^2(\mathbf{s})$ because of partition label switching throughout the MCMC. For each model, Brier scores were were averaged over all sites and days to obtain a single Brier score for each dataset. At a particular threshold or quantile level, the model that fits the best is the one with the lowest score. We then compute the relative (to Gaussian) Brier scores (see Section 5.3) to compare each model.

6.2   Results

The results suggest that the skew-t, thresholded, partitioned, and time series models all give an improvement in predictions over the Gaussian model, whereas the max-stable method results in relative Brier scores between 1.07 and 1.15 indicating poorer performance than the Gaussian model. The plots in Figure 4 show the relative Brier scores for time-series and non-time-series models, using $K = 1, 7$, and 15 knots at thresholds $T = 0, 50$, and 75 ppb. Most of the models perform similarly across all the Brier scores; however, for single-partition models without thresholding, performance tends to diminish in the extreme quantiles. The results also suggest that thresholding improves performance for estimates in the extreme quantiles. Both plots have similar features suggesting that most settings do reasonably well. In particular, for all extreme quantiles, selecting a moderate number of knots (e.g. $K = 5, \ldots, 10$) tends to give the best results. Table 1 shows the best two models for selected extreme quantiles.
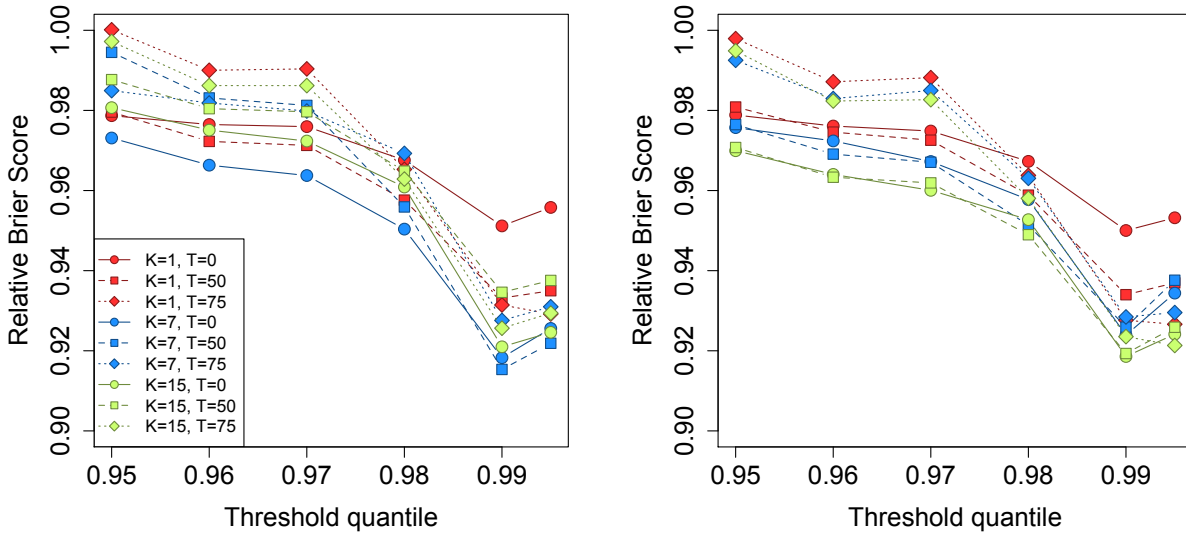
18

Figure 4: Relative Brier scores for time-series models (left) and non-time-series models (right). Relative brier score for the max-stable model is between 1.07 and 1.15

We illustrate the predictive capability of our model in Figure 5 by plotting the 99th quantile of the posterior predictive density for July in South Carolina and Georgia. We fit the model using four methods, two reference and two that performed better. These four methods are

1. Gaussian (reference)

2. Skew-t, $K = 1$ knot, $T = 0$, no time series (reference)

3. Skew-t, $K = 5$ knots, $T = 50$, no time series (comparison)

4. Symmetric-t, $K = 10$ knots, $T = 75$, time series (comparison).

In the bottom two plots, we plot the differences between method 4 and methods 1 and 2. The most noticeable differences between the reference methods and the comparison methods is that the comparison methods tend to give higher estimates of the 99th quantile along the I-85 corridor between Charlotte and Atlanta.

19

Table 1: Top two performing models for ozone analysis at extreme quantiles with Relative Brier score

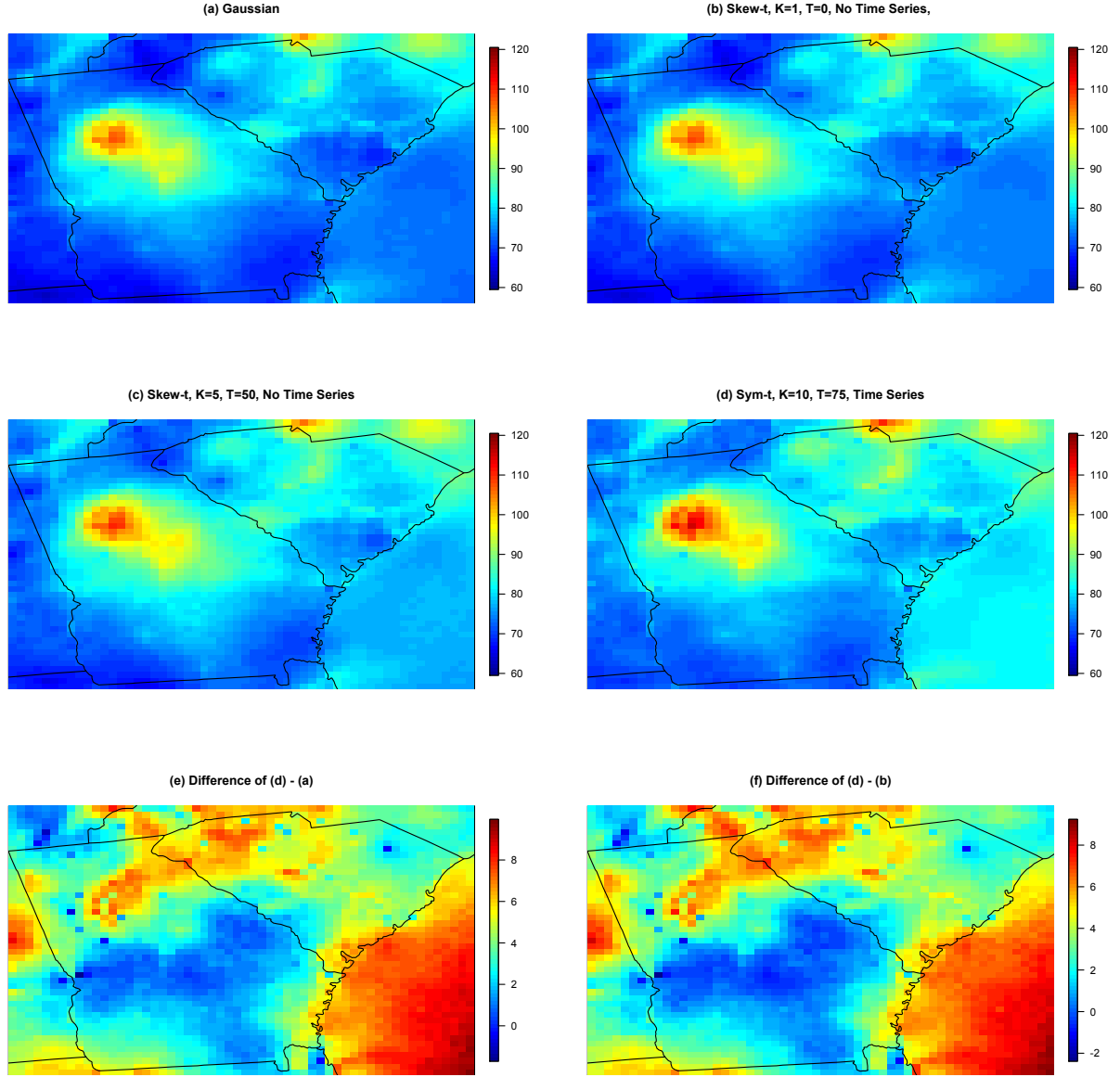|	1st				2nd			
$q(0.90)$	No time series	$K=7$	$T=0$	BS: 0.980	No time series	$K=9$	$T=0$	BS: 0.980
$q(0.95)$	No time series	$K=15$	$T=50$	BS: 0.970	No time series	$K=9$	$T=50$	BS: 0.970
$q(0.98)$	No time series	$K=5$	$T=50$	BS: 0.945	No time series	$K=10$	$T=50$	BS: 0.946
$q(0.99)$	Time series	$K=10$	$T=75$	BS: 0.912	Time series	$K=6$	$T=75$	BS: 0.913
$q(0.995)$	Time series	$K=6$	$T=75$	BS: 0.917	Time series	$K=10$	$T=75$	BS: 0.918

Figure 5: (a) – (d) give give the posterior predictive $\widehat{q}(0.99)$ for the month of July under four different models, (e) gives the difference between $\widehat{q}(0.99)$ in plots (d) and (a), (f) gives the difference between $\widehat{q}(0.99)$ in plots (d) and (b).

7 Discussion

In this paper we propose a new approach for spatitemporal modeling of extreme values. The proposed model gives flexible tail behavior, demonstrates asymptotic dependence for observations at sites that are near to one another, and has computation on the order of Gaussian models for large space-time datasets. In the simulation study, we demonstrate that this model shows statistically significant improvements over a naïve Gaussian approach. In both the simulation study, and the application to ozone data, we find that incorporating a partition in the model improves extreme prediction. Furthermore the results from the data analysis suggest that thresholding can improve performance when predicting in the extreme tails of the data.

This model presents new avenues for future research. One possibility is the implementation of a different partition structure. We choose to define the random effects for a site by using an indicator function based on closeness to a knot. However, this indicator function could be replaced by kernel function that would allow for multiple knots to impact each site, with the weight of each knot to be determined by some characteristic such as distance. Another area that should be explored is the temporal dependence in the model. Instead of implementing a time series on the random effects, a three-dimensional covariance structure on the residuals could be implemented to address temporal dependence. Finally, we acknowledge that by specifying the number of knots, we may be underestimating the uncertainty in the model. This could be incoporated by treating the number of knots as a model parameter instead of fixing it to be a specific value.

316 Acknowledgments

317 A Appendices

318 A.1 MCMC details

319 The MCMC sampling for the model 4.1 is done using R (http://www.r-project.org). Whenever possible,

320 we select conjugate priors (see Appendix A.2); however, for some of the parameters, no conjugate prior

321 distributions exist. When no conjugate prior distribution exists, we use a random walk Metropolis Hastings

322 update step. In each Metropolis Hastings update, we tune the algorithm to give acceptance rates near 0.40.

Spatial knot locations

324 For each day, we update the spatial knot locations, $\mathbf{w}_1, \ldots, \mathbf{w}_K$, using a Metropolis Hastings block up-

325 date. Because the spatial domain is bounded, we generate candidate knots using the transformed knots

326 $\mathbf{w}_1^*, \ldots, \mathbf{w}_K^*$ (see section 3.3) and a random walk bivariate Gaussian candidate distribution

$$\mathbf{w}_k^{*(c)} \sim \mathrm{N}(\mathbf{w}_k^{*(r-1)}, s^2 I_2)$$

327 where $\mathbf{w}_k^{*(r-1)}$ is the location for the transformed knot at MCMC iteration $r-1$, s is a tuning parameter,

328 and I_2 is an identity matrix. After candidates have been generated for all K knots, the acceptance ratio is

$$R = \left\{ \frac{l[Y_t(\mathbf{s}|\mathbf{w}_1^{(c)}, \ldots, \mathbf{w}_K^{(c)}, \ldots)]}{l[Y_t(\mathbf{s}|\mathbf{w}_1^{(r-1)}, \ldots, \mathbf{w}_K^{(r-1)}, \ldots)]} \right\} \times \left\{ \frac{\prod_{k=1}^K \phi(\mathbf{w}_k^{(c)})}{\prod_{k=1}^K \phi(\mathbf{w}_k^{(r-1)})} \right\} \times \left\{ \frac{\prod_{k=1}^K p(\mathbf{w}_k^{*(c)})}{\prod_{k=1}^K p(\mathbf{w}_k^{*(r-1)})} \right\}$$

329 where l is the likelihood given in (18), and $p(\cdot)$ is the prior either taken from the time series given in (3.3)

330 or assumed to be uniform over $\mathcal{D}$. The candidate knots are accepted with probability $\min\{R, 1\}$.

22

Spatial random effects

If there is no temporal dependence amongst the observations, we use a Gibbs update for z_{tk}, and the posterior

distribution is given in A.2. If there is temporal dependence amongst the observations, then we update z_{tk}

using a Metropolis Hastings update. Because this model uses $|z_{tk}|$, we generate candidate random effects

using the z_{tk}^* (see Section 3.3) and a random walk Gaussian candidate distribution

$$z_{tk}^{*\,(c)} \sim \text{N}(z_{tk}^{*\,(r-1)}, s^2)$$

where $z_{tk}^{*\,(r-1)}$ is the value at MCMC iteration $r-1$, and s is a tuning parameter. The acceptance ratio is

$$R = \left\{ \frac{l[Y_t(\mathbf{s})|z_{tk}^{(c)}, \ldots]}{l[Y_t(\mathbf{s})|z_{tk}^{(r-1)}]} \right\} \times \left\{ \frac{p[z_{tk}^{(c)}]}{p[z_{tk}^{(r-1)}]} \right\}$$

where $p[\cdot]$ is the prior taken from the time series given in Section 3.3. The candidate is accepted with

probability $\min\{R, 1\}$.

Variance terms

When there is more than one site in a partition, then we update σ_{tk}^2 using a Metropolis Hastings update.

First, we generate a candidate for σ_{tk}^2 using an $\text{IG}(a^*/s, b^*/s)$ candidate distribution in an independence

Metropolis Hastings update where $a^* = (n_{tk}+1)/2 + a$, $b^* = [Y_{tk}^T \Sigma_{tk}^{-1} Y_{tk} + z_{tk}^2]/2 + b$, n_{tk} is the number

of sites in partition k on day t, and Y_{tk} and Σ_{tk}^{-1} are the observations and precision matrix for partition k on

day t. The acceptance ratio is

$$R = \left\{ \frac{l[Y_t(\mathbf{s})|\sigma_{tk}^{2\,(c)}, \ldots]}{l[Y_t(\mathbf{s})|\sigma_{tk}^{2\,(r-1)}]} \right\} \times \left\{ \frac{l[z_{tk}|\sigma_{tk}^{2\,(c)}, \ldots]}{l[z_{tk}|\sigma_{tk}^{2\,(r-1)}, \ldots]} \right\} \times \left\{ \frac{p[\sigma_{tk}^{2\,(c)}]}{p[\sigma_{tk}^{2\,(r-1)}]} \right\} \times \left\{ \frac{c[\sigma_{tk}^{2\,(r-1)}]}{c[\sigma_{tk}^{2\,(c)}]} \right\}$$

345 where $p[\cdot]$ is the prior either taken from the time series given in Section 3.3 or assumed to be IG(a, b), and

346 $c[\cdot]$ is the candidate distribution. The candidate is accepted with probability $\min\{R, 1\}$.

Spatial covariance parameters

348 We update the three spatial covariance parameters, $\log(\rho)$, $\log(\nu)$, γ, using a Metropolis Hastings block

349 update step. First, we generate a candidate using a random walk Gaussian candidate distribution

$$\log(\rho)^{(c)} \sim \text{N}(\log(\rho)^{(r-1)}, s^2)$$

350 where $\log(\rho)^{(r-1)}$ is the value at MCMC iteration $r - 1$, and s is a tuning parameter. Candidates are

351 generated for $\log(\nu)$ and γ in a similar fashion. The acceptance ratio is

$$R = \left\{ \frac{\prod_{t=1}^{T} l[Y_t(\mathbf{s})|\rho^{(c)}, \nu^{(c)}, \gamma^{(c)}, \ldots]}{\prod_{t=1}^{T} l[Y_t(\mathbf{s})|\rho^{(r-1)}, \nu^{(r-1)}, \gamma^{(r-1)}, \ldots]} \right\} \times \left\{ \frac{p[\rho^{(c)}]}{p[\rho^{(r-1)]}} \right\} \times \left\{ \frac{p[\nu^{(c)}]}{p[\nu^{(r-1)}]} \right\} \times \left\{ \frac{p[\gamma^{(c)}]}{p[\gamma^{(r-1)}]} \right\}.$$

352 All three candidates are accepted with probability $\min\{R, 1\}$.

A.2 Posterior distributions

Conditional posterior of $z_{tk} \mid \ldots$

355 If knots are independent over days, then the conditional posterior distribution of $|z_{tk}|$ is conjugate. For

356 simplicity, drop the subscript t, let $\tilde{z}_{tk} = |z_{tk}|$, and define

$$R(\mathbf{s}) = \begin{cases} Y(\mathbf{s}) - X(\mathbf{s})\beta & s \in P_l \\[2em] Y(\mathbf{s}) - X(\mathbf{s})\beta - \lambda\tilde{z}(\mathbf{s}) & s \notin P_l \end{cases}$$

24

Let

$$R_1 = \text{the vector of } R(\mathbf{s}) \text{ for } s \in P_l$$

$$R_2 = \text{the vector of } R(\mathbf{s}) \text{ for } s \notin P_l$$

$$\Omega = \Sigma^{-1}.$$

Then

$$\pi(z_l | \dots) \propto \exp\left\{ -\frac{1}{2} \left[\begin{pmatrix} R_1 - \lambda \tilde{z}_l \mathbf{1} \\ R_2 \end{pmatrix}^T \begin{pmatrix} \Omega_{11} & \Omega_{12} \\ \Omega_{21} & \Omega_{22} \end{pmatrix} \begin{pmatrix} R_1 - \lambda \tilde{z}_l \mathbf{1} \\ R_2 \end{pmatrix} + \frac{\tilde{z}_l^2}{\sigma_l^2} \right] \right\} I(z_l > 0)$$

$$\propto \exp\left\{ -\frac{1}{2} \left[\Lambda_l \tilde{z}_l^2 - 2\mu_l \tilde{z}_l \right] \right\}$$

where

$$\mu_l = \lambda (R_1^T \Omega_{11} + R_2^T \Omega_{21}) \mathbf{1}$$

$$\Lambda_l = \lambda^2 \mathbf{1}^T \Omega_{11} \mathbf{1} + \frac{1}{\sigma_l^2}.$$

Then $\tilde{Z}_l | \dots \sim N_{(0,\infty)}(\Lambda_l^{-1} \mu_l, \Lambda_l^{-1})$

25

Conditional posterior of $\beta \mid \ldots$

Let $\beta \sim \mathrm{N}_p(0, \Lambda_0)$ where Λ_0 is a precision matrix. Then

$$\pi(\beta \mid \ldots) \propto \exp \left\{ -\frac{1}{2} \beta^T \Lambda_0 \beta - \frac{1}{2} \sum_{t=1}^{T} [\mathbf{Y}_t - X_t \beta - \lambda|z_t|]^T \Omega [\mathbf{Y}_t - X_t \beta - \lambda|z_t|] \right\}$$

$$\propto \exp \left\{ -\frac{1}{2} \left[\beta^T \Lambda_\beta \beta - 2 \sum_{t=1}^{T} [\beta^T X_t^T \Omega (\mathbf{Y}_t - \lambda|z_t|)] \right] \right\}$$

$$\propto \mathrm{N}(\Lambda_\beta^{-1} \mu_\beta, \Lambda_\beta^{-1})$$

where

$$\mu_\beta = \sum_{t=1}^{T} \left[X_t^T \Omega (\mathbf{Y}_t - \lambda|z_t|) \right]$$

$$\Lambda_\beta = \Lambda_0 + \sum_{t=1}^{T} X_t^T \Omega X_t.$$

Conditional posterior of $\sigma^2 \mid \ldots$

In the case where $L = 1$ and temporal dependence is negligible, then σ^2 has a conjugate posterior distribution. Let $\sigma_t^2 \overset{iid}{\sim} \mathrm{IG}(\alpha_0, \beta_0)$. For simplicity, drop the subscript t. Then

$$\pi(\sigma^2 \mid \ldots) \propto (\sigma^2)^{-\alpha_0 - 1/2 - n/2 - 1} \exp \left\{ -\frac{\beta_0}{\sigma^2} - \frac{|z|^2}{2\sigma^2} - \frac{(\mathbf{Y} - \boldsymbol{\mu})^T \Sigma^{-1} (\mathbf{Y} - \boldsymbol{\mu})}{2\sigma^2} \right\}$$

$$\propto (\sigma^2)^{-\alpha_0 - 1/2 - n/2 - 1} \exp \left\{ -\frac{1}{\sigma^2} \left[\beta_0 + \frac{|z|^2}{2} + \frac{1}{2} (\mathbf{Y} - \boldsymbol{\mu})^T \Sigma^{-1} (\mathbf{Y} - \boldsymbol{\mu}) \right] \right\}$$

$$\propto \mathrm{IG}(\alpha^*, \beta^*)$$

where

$$\alpha^* = \alpha_0 + \frac{1}{2} + \frac{n}{2}$$

$$\beta^* = \beta_0 + \frac{|z|^2}{2} + \frac{1}{2}(\mathbf{Y} - \boldsymbol{\mu})^T \Sigma^{-1} (\mathbf{Y} - \boldsymbol{\mu}).$$

368 In the case that $L > 1$, a random walk Metropolis Hastings step will be used to update σ_{lt}^2.

369 **Conditional posterior of $\lambda \mid \ldots$**

370 For convergence purposes we model $\lambda = \lambda_1 \lambda_2$ where

$$\lambda_1 = \begin{cases} +1 & \text{w.p.0.5} \\ \\ -1 & \text{w.p.0.5} \end{cases} \tag{22}$$

$$\lambda_2^2 \sim IG(\alpha_\lambda, \beta_\lambda). \tag{23}$$

$$\tag{24}$$

371 Then

$$\pi(\lambda_2 \mid \ldots) \propto \lambda_2^{2(-\alpha_\lambda - 1)} \exp\left\{-\frac{\beta_\lambda}{\lambda_2^2}\right\} \prod_{t=1}^{T} \prod_{k=1}^{K} \frac{1}{\lambda_2} \exp\left\{-\frac{z_{tk}^2}{2\lambda_2^2 \sigma_{tk})^2}\right\}$$

$$\propto \lambda_2^{2(-\alpha_\lambda - kt - 1)} \exp\left\{-\frac{1}{\lambda_2^2}\left[\beta_\lambda + \frac{z^2}{2\sigma_{tk}^2}\right]\right\}$$

372 Then $\lambda_2 \mid \ldots \sim IG(\alpha_\lambda + kt, \beta_\lambda + \frac{z^2}{2\sigma_{tk}^2}$

A.3 Proof that $\lim_{h\to\infty} \pi(h) = 0$

Let $N(A)$ be the number of knots in A, the area between sites $\mathbf{s}_1$ and $\mathbf{s}_2$. Consider a spatial Poisson process with intensity $\mu(A)$. So,

$$P[N(A) = k] = \frac{\mu(A)^k \exp\{-\mu(A)\}}{k!}.$$

Then for any finite k, $\lim_{h\to\infty} P[N(A) = k] = 0$ because $\lim_{h\to\infty} \mu(A) = \infty$. With each additional knot in A, the chance that $\mathbf{s}_1$ and $\mathbf{s}_2$ will be be in the same partition will decrease, because partition membership is defined by the closest knot to a site. Therefore, $\lim_{h\to\infty} \pi(h) = 0$.

A.4 Skew-t distribution

Univariate extended skew-t distribution

We say that Y follow a univariate extended skew-t distribution with location $\xi \in \mathcal{R}$, scale $\omega > 0$, skew parameter $\alpha \in \mathcal{R}$, extended parameter $\tau \in \mathcal{R}$, and degrees of freedom ν if has distribution function

$$f_{\mathrm{EST}}(y) = \omega^{-1} \frac{f_T(z;\nu)}{F_T(\tau/\sqrt{1+\alpha^2};\nu)} F_T\left[(\alpha z + \tau)\sqrt{\frac{\nu+1}{\nu+z^2}}; 0, 1, \nu+1\right] \tag{25}$$

where $f_T(t;\nu)$ is a univariate Student's t with ν degrees of freedom, $F_T(t;\nu) = P(T < t)$, and $z = (y - \xi)/\omega$. In the case that $\tau = 0$, then Y follows a univariate skew-t distribution.

Multivariate skew-t distribution

If $\mathbf{Z} \sim \mathrm{ST}_d(0, \bar{\boldsymbol{\Omega}}, \boldsymbol{\alpha}, \eta)$ is a d-dimensional skew-t distribution, and $\mathbf{Y} = \xi + \boldsymbol{\omega}\mathbf{Z}$, where $\boldsymbol{\omega} = \mathrm{diag}(\omega_1, \ldots, \omega_d)$, then the density of Y at y is

$$f_y(\mathbf{y}) = det(\boldsymbol{\omega})^{-1} f_z(\mathbf{z}) \tag{26}$$

where

$$f_z(\mathbf{z}) = 2t_d(\mathbf{z}; \bar{\boldsymbol{\Omega}}, \eta) T \left[\boldsymbol{\alpha}^T \mathbf{z} \sqrt{\frac{\eta + d}{\nu + Q(\mathbf{z})}}; \eta + d \right] \tag{27}$$

$$\mathbf{z} = \boldsymbol{\omega}^{-1}(\mathbf{y} - \xi) \tag{28}$$

where $t_d(\mathbf{z}; \bar{\boldsymbol{\Omega}}, \eta)$ is a d-dimensional Student's t-distribution with scale matrix $\bar{\boldsymbol{\Omega}}$ and degrees of freedom η, $Q(z) = \mathbf{z}^T \bar{\Omega}^{-1} \mathbf{z}$ and $T(\cdot; \eta)$ denotes the univariate Student's t distribution function with η degrees of freedom (**?**).

Extremal dependence

For a bivariate skew-t random variable $\mathbf{Y} = [Y(\mathbf{s}), Y(\mathbf{t})]^T$, the $\chi(h)$ statistic (Padoan, 2011) is given by

$$\chi(h) = \bar{F}_{\mathrm{EST}} \left\{ \frac{[x_1^{1/\eta} - \varrho(h)]\sqrt{\eta + 1}}{\sqrt{1 - \varrho(h)^2}}; 0, 1, \alpha_1, \tau_1, \eta + 1 \right\} + \bar{F}_{\mathrm{EST}} \left\{ \frac{[x_2^{1/\eta} - \varrho(h)]\sqrt{\eta + 1}}{\sqrt{1 - \varrho(h)^2}}; 0, 1, \alpha_2, \tau_2, \eta + 1 \right\},$$

$$\tag{29}$$

where $\bar{F}_{\mathrm{EST}}$ is the univariate survival extended skew-t function with zero location and unit scale, $\varrho(h) = \mathrm{cor}(y_1, y_2)$, $\alpha_j = \alpha_i \sqrt{1 - \varrho^2}$, $\tau_j = \sqrt{\eta + 1}(\alpha_j + \alpha_i \varrho)$, and $x_j = F_T(\bar{\alpha}_i \sqrt{\eta + 1}; 0, 1, \eta) / F_T(\bar{\alpha}_j \sqrt{\eta + 1}; 0, 1, \eta)$ with $j = 1, 2$ and $i = 2, 1$ and where $\bar{\alpha}_j = (\alpha_j + \alpha_i \varrho) / \sqrt{1 + \alpha_i^2[1 - \varrho(h)^2]}$.

Proof that $\lim_{h \to \infty} \chi(h) > 0$

398 Consider the bivariate distribution of $\mathbf{Y} = [Y(\mathbf{s}), Y(\mathbf{t})]^T$, with $\varrho(h)$ given by (3). So, $\lim_{h \to \infty} \varrho(h) = 0$.

399 Then

$$\lim_{h \to \infty} \chi(h) = \bar{F}_{\mathrm{EST}} \left\{ \sqrt{\eta + 1}; 0, 1, \alpha_1, \tau_1, \eta + 1 \right\} + \bar{F}_{\mathrm{EST}} \left\{ \sqrt{\eta + 1}; 0, 1, \alpha_2, \tau_2, \eta + 1 \right\}. \tag{30}$$

400 Because the extended skew-t distribution is not bounded above, for all $\bar{F}_{\mathrm{EST}}(x) = 1 - F_{\mathrm{EST}} > 0$ for all

401 $x < \infty$. Therefore, for a skew-t distribution, $\lim_{h \to \infty} \chi(h) > 0$.

A.5 Simulation study pairwise difference results

403 The following tables show the methods that have significantly different Brier scores when using a Wilcoxon-

404 Nemenyi-McDonald-Thompson test. In each column, different letters signify that the methods have signifi-

405 cantly different Brier scores. For example, there is significant evidence to suggest that method 1 and method

406 4 have different Brier scores at $q(0.90)$, whereas there is not significant evidence to suggest that method 1

407 and method 2 have different Brier scores at $q(0.90)$. In each table group A represents the group with the

408 lowest Brier scores. Groups are significant with a familywise error rate of $\alpha = 0.05$.

Table 2: Setting 1 – Gaussian marginal, $K = 1$ knot

	$q(0.90)$	$q(0.95)$	$q(0.98)$	$q(0.99)$
Method 1	A	A	A	A
Method 2	A B	A B	A	A
Method 3	C	C	C	B
Method 4	B	B	B	B
Method 5	C	C	C	B

Table 3: Setting 2 – Skew-t marginal, $K = 1$ knot

	$q(0.90)$	$q(0.95)$	$q(0.98)$	$q(0.99)$
Method 1	B	B	B	B
Method 2	A	A	A	A
Method 3	B	B	B	A B
Method 4	B	B	B	B
Method 5	C	C	C	C

Table 4: Setting 3 – Skew-t marginal, $K = 5$ knots

	$q(0.90)$	$q(0.95)$	$q(0.98)$	$q(0.99)$
Method 1	B	B	B	C
Method 2	B	B	B	B C
Method 3	A	A	B	C
Method 4	A	A	A	A B
Method 5	A	A	A	A

Table 5: Setting 4 – Max-stable

	$q(0.90)$	$q(0.95)$	$q(0.98)$	$q(0.99)$
Method 1	A	A	A B	C
Method 2	B	A B	A	A B
Method 3	C	B C	A B	A
Method 4	D	D	C	C
Method 5	C D	C	B	B C

Table 6: Setting 5 – Transformation below $T = q(0.80)$

	$q(0.90)$	$q(0.95)$	$q(0.98)$	$q(0.99)$
Method 1	C	B	C	C
Method 2	B	B	A B	A B
Method 3	A	A	A	A
Method 4	B C	B	B	B C
Method 5	B C	B	C	C

References

Blanchet, J. and Davison, A. C. (2011) Spatial modeling of extreme snow depth. *The Annals of Applied Statistics*, **5**, 1699–1725. URLhttp://projecteuclid.org/euclid.aoas/1318514282.

Coles, S. (2001) *An Introduction to Statistical Modeling of Extreme Values*. Lecture Notes in Control and Information Sciences. London: Springer. URLhttps://books.google.com/books?id=2nugUEaKqFEC.

Coles, S. G. and Tawn, J. A. (1991) Modelling Extreme Multivariate Events. *Journal of the Royal Statistical Society: Series B (Methodological)*, **53**, 377–392. URLhttp://www.jstor.org/stable/10.2307/2345748.

Cooley, D., Cisewski, J., Erhardt, R. J., Mannshardt, E., Omolo, B. O. and Sun, Y. (2012) A survey of spatial extremes: Measuring spatial dependence and modeling spatial effects. *REVSTAT*, **10**, 135–165. URLhttp://www.ine.pt/revstat/pdf/rs120106.pdf.

Davison, A. C. and Gholamrezaee, M. M. (2012) Geostatistics of extremes.

DuMouchel, W. H. (1983) Estimating the stable index α in order to measure tail thickness: a critique. *The Annals of Statistics*, **11**, 1019–1031. URLhttp://www.jstor.org/stable/2241294.

Engelke, S., Malinowski, A., Kabluchko, Z. and Schlather, M. (2014) Estimation of Hüsler-Reiss distributions and Brown-Resnick processes. *Journal of the Royal Statistical Society. Series B: Statistical Methodology*, 239–265.

Genton, M. G. (2004) *Skew-Elliptical Distributions and Their Applications: A Journey Beyond Normality*. Statistics (Chapman & Hall/CRC). Taylor & Francis. URLhttp://books.google.com/books?id=R9hBnwEACAAJ.

Gneiting, T. and Raftery, A. E. (2007) Strictly Proper Scoring Rules, Prediction, and Estimation. *Journal of the American Statistical Association*, **102**, 359–378. URLhttp://www.tandfonline.com/doi/abs/10.1198/016214506000001437.

de Haan, L. and Ferreira, A. (2006) *Extreme Value Theory: An Introduction*. Springer Series in Operations Research and Financial Engineering. Springer. URLhttps://books.google.com/books?id=catZCl17d7gC.

Huser, R. (2013) *Statistical Modeling and Inference for Spatio-Temporal Extremes*. Ph.D. thesis. URLhttp://infoscience.epfl.ch/record/188557/files/EPFL_TH5946.pdf.

Huser, R. and Davison, A. C. (2014) Space-time modelling of extreme events. *Journal of the Royal Statistical Society: Series B (Statistical Methodology)*, **76**, 439–461. URLhttp://arxiv.org/abs/1201.3245 http://doi.wiley.com/10.1111/rssb.12035.

Kim, H.-M., Mallick, B. K. and Holmes, C. C. (2005) Analyzing Nonstationary Spatial Data Using Piecewise Gaussian Processes. *Journal of the American Statistical Association*, **100**, 653–668.

Opitz, T. (2013) Extremal t processes: Elliptical domain of attraction and a spectral representation. *Journal of Multivariate Analysis*, **122**, 409–413. URLhttp://dx.doi.org/10.1016/j.jmva.2013.08.008.

Padoan, S. A. (2011) Multivariate extreme models based on underlying skew- and skew-normal distributions. *Journal of Multivariate Analysis*, **102**, 977–991. URLhttp://linkinghub.elsevier.com/retrieve/pii/S0047259X11000157.

Padoan, S. A., Ribatet, M. and Sisson, S. A. (2010) Likelihood-Based Inference for

Max-Stable Processes. *Journal of the American Statistical Association*, **105**, 263–277. URLhttp://www.tandfonline.com/doi/abs/10.1198/jasa.2009.tm08577.

Reich, B. J. and Shaby, B. A. (2012) A hierarchical max-stable spatial model for extreme precipitation. *The Annals of Applied Statistics*, **6**, 1430–1451. URLhttp://projecteuclid.org/euclid.aoas/1356629046.

Thibaud, E., Mutzner, R. and Davison, a. C. (2013) Threshold modeling of extreme spatial rainfall. *Water Resources Research*, **49**, 4633–4644.

Thibaud, E. and Opitz, T. (2013) Efficient inference and simulation for elliptical Pareto processes. 1–19.

Wadsworth, J. L. and Tawn, J. a. (2012) Dependence modelling for spatial extremes. *Biometrika*, **99**, 253–272.

— (2013) Efficient inference for spatial extreme value processes associated to log-Gaussian random functions. *Biometrika*, **101**, 1–15. URLhttp://biomet.oxfordjournals.org/cgi/doi/10.1093/biomet/ast042.

Zhang, H. and El-Shaarawi, A. (2010) On spatial skewGaussian processes and applications. *Environmetrics*, **21**, 33–47. URLhttp://onlinelibrary.wiley.com/doi/10.1002/env.982/abstract.